

Article

The Design of Façade-Integrated Vertical Greenery to Mitigate the Impacts of Extreme Weather: A Case Study from Hong Kong

Changying Xiang * and Lulu Tao

Division of Integrative Systems and Design, The Hong Kong University of Science and Technology, Hong Kong; lulutao@ust.hk

* Correspondence: changyingx@ust.hk

Abstract: Vertical greenery not only helps to cool the surfaces of buildings but, more importantly, it can also mitigate the Urban Heat Island effect. The growth of vertical greenery is highly dependent on ongoing maintenance, such as irrigation. Wind-driven rain serves as a natural source of irrigation for vertical greenery. Wind-driven rain simulation was conducted on a typical high-density and high-rise case in Hong Kong to first classify the wind-driven rain harvesting potential on the façade with very high, high, moderate, low, and very low levels. Then, Scenario 1 (very high potential), Scenario 2 (very high + high potential), and Scenario 3 (very high + high + moderate potential) regarding vertical greenery in locations with three levels of wind-driven rain harvesting potential were simulated in ENVI-met to assess its Urban Heat Island mitigation effect. The maximum temperature reduction on the street occurs between 12 p.m. and 3 p.m., indicating the greatest mitigation of the Urban Heat Island effect. Scenario 1, Scenario 2, and Scenario 3 achieve a maximum temperature reduction of 0.76 °C, 0.88 °C, and 1.06 °C, respectively, during this time period.

Keywords: façade-integrated vertical greenery; climate-resilient; high-density cities; Urban Heat Island effect; Global Boiling; climate change; sponge city; architectural design



Citation: Xiang, C.; Tao, L. The Design of Façade-Integrated Vertical Greenery to Mitigate the Impacts of Extreme Weather: A Case Study from Hong Kong. *Buildings* **2023**, *13*, 2865. <https://doi.org/10.3390/buildings13112865>

Academic Editor: Antonio Caggiano

Received: 20 October 2023

Revised: 10 November 2023

Accepted: 14 November 2023

Published: 16 November 2023



Copyright: © 2023 by the authors. Licensee MDPI, Basel, Switzerland. This article is an open access article distributed under the terms and conditions of the Creative Commons Attribution (CC BY) license (<https://creativecommons.org/licenses/by/4.0/>).

1. Introduction

1.1. Background

Climate change has resulted in more extreme weather that affects all countries all over the world [1]. Large cities with high populations are more vulnerable to uncertainty and destructive weather such as frequent heavy rainfalls, extreme heatwaves, etc. [2].

Hong Kong (22°16'50" N, 114°10'20" E) has a monsoon-influenced subtropical climate. In addition to increasing threats from heat waves, heavy rainfall brought by tropical cyclones have become more frequent in recent years, which has caused the most significant economic loss in Hong Kong [3]. The statistical data showed a significant 5% increase in the rate of the annual number of heavy rain days [4]. This past September, Super Typhoon Saola cast phenomenal rainstorms in Hong Kong and led to more than 16 h of Black Rainstorm Warnings (triggered when precipitation that exceeds 70 mm in an hour is expected), the longest record since 1992 [5]. Urban flash floods are associated with heavy rainstorms. Therefore, it is essential to enhance the cities' rainwater management capacity to tackle the increasingly frequent and extreme precipitation [6,7].

With the 'hottest month on record' of July 2023 serving as an alert that 'the era of global warming has ended', we are now entering the era of 'Global Boiling' [8]. High-density cities suffer more due to record-breaking hot weather. Typically, urban areas with a higher density of buildings tend to have poorer ventilation conditions and experience a more pronounced Urban Heat Island (UHI) effect [9,10]. Studies in some high-density urban regions show that up to 5 °C UHI intensity can be detected [11], which creates threats to both citizens' health and well-being (such as extreme heat-related mortality) [12,13]. In the summer of 2022, nearly 62,000 people died from record-breaking heat in Europe [14].

In August 2023, Hong Kong experienced a recorded average temperature of 29.7 °C, the highest on record in almost the last one and a half centuries [15]. Heat waves in the summer are not occasional events: in the past 30 years, there was a dramatic increase in observed very hot days (daily maximum air temperature ≥ 33 °C) and very hot nights (minimum air temperature ≥ 28 °C) in Hong Kong, while most of the very hot days happened during July, August, and September every year [16] (Figure 1). The increasing number of very hot days also led to higher cooling energy consumption of buildings [17]. Studies showed that, in the urban context of Hong Kong, a 1 °C increase in ambient temperature would result in an increase in electricity consumption of 9.2% in the domestic sector, 3.0% in the commercial sector, and 2.4% in the industrial sector [18]. Mass-scale solutions to mitigate overheating in cities are urgently needed.

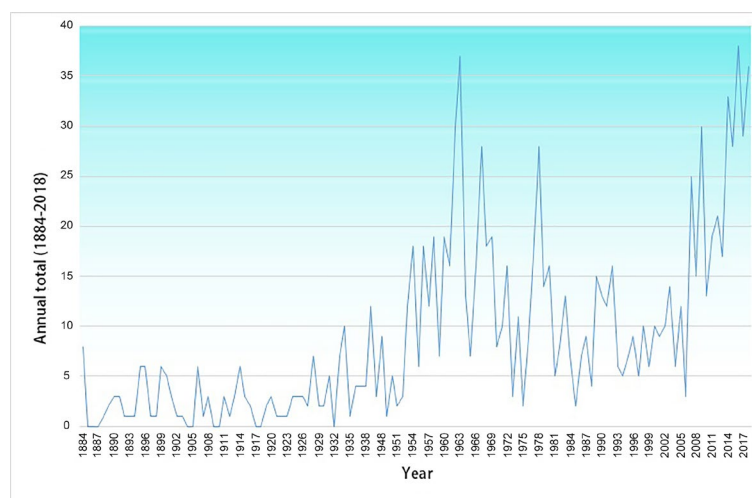


Figure 1. The number of very hot days observed at the Hong Kong Observatory since 1884, excluding 1940–1946. From the Hong Kong Observatory.

Urban greenery can also provide a stormwater buffer for the cities [19]. An analysis of over 2000 green roof cases across 21 countries showed that the average runoff retention (RR) rate was 62% (62% of the rainfall was retained) [20]. Greenery can absorb and purify a certain amount of precipitation on heavy rainy days and then release the water gradually to reduce urban flash floods, providing the cities with a “sponge” capacity for rainwater management [21]. Researchers from TU/e conducted a module-scale study to investigate the VGS’s rainwater buffer capacity using experimental tests of two types of living wall modules for two months, and the results showed that up to 33% of the rainfall reaching a horizontal plane could be retained with the same area of a living wall [22] (Figure 2). To further analyze precipitation on façades, the wind-driven rain effect (WDR), which means the conjunction of rain and wind [23,24], needs to be considered because it is a main contributing source of falling precipitation on façades, causing threats to buildings’ hygrothermal performance and durability [25,26].

On the other hand, urban greenery such as rooftop greenery and vertical greenery systems (VGSs) can be an effective method to mitigate the UHI effect [11,27]. In high-density urban regions where roof areas are limited, the urban cooling potential of VGSs should be exploited to maximize their contribution. A literature review study showed that, in all the climate zones studied, the implementation of green walls could lead to a reduction in building energy demand for heating and cooling by approximately 16.5% and 51%, respectively. Additionally, they can help mitigate the UHI effect by up to approximately 5 °C (while in high-density urban contexts, the cooling effects could be up to 8 °C) [28].

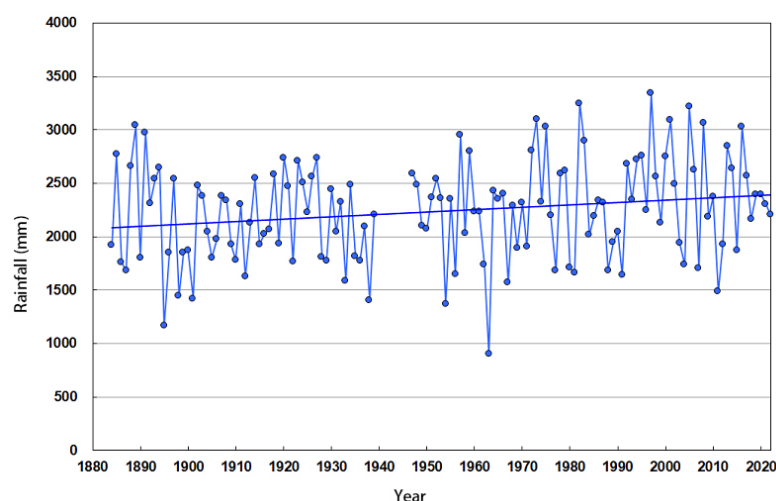


Figure 2. Annual number of heavy rain days in Hong Kong (1884–2022). From the Hong Kong Observatory.

1.2. Literature Review

1.2.1. Review of Vertical Greenery Studies

A great number of studies have proved the benefits of greenery in urban environments [29–32]. Vertical greenery's shading effects, insulation capacity, and evaporation process can regulate temperature, radiation, airflow, humidity, etc., thus changing the heat loss of building façades and mitigating thermal comfort, UHI, and the microclimate. For instance, D.H.S. Duarte et al. [33] assessed the effects of cooling and outdoor thermal comfort of greenery in an urban environment to counterbalance urban warming effects resulting from an increase in built density in a subtropical climate. Four scenarios: (1) base case: only towers, (2) towers and central parts, (3) towers and pocket parks, and (4) towers and street trees, were simulated using ENVI-met after validation using field measurements. Based on the air temperature, mean radiant temperature, and surface temperature data, the Physiological Equivalent Temperature (PET) and Temperature of Equivalent Perception (TEP) were calculated to assess outdoor thermal comfort. Similar to Moren M. et al.'s conclusions [34], their study proved that air temperature differences in scenario (4) became more significant up to 0.6 °C during extremely warm summers compared with scenario (1). The finest thermal comfort was found in scenario (2) due to decreasing radiant temperature. Morakinyo T. et al. [35] conducted an ENVI-met simulation to investigate the impact of vertical greenery on air cooling and thermal comfort in parametric neighborhood models with different densities. Both the ideal parametric model (regular building form, no podium) and realistic Hong Kong building form (building block with podium) with different greenery façade ratios or orientations yielded eleven scenarios with parameters including urban density, the greened façade ratio (GFR), and greened façade orientation. Their conclusions indicated that 30–50% of the façades in the high-density urban setting of Hong Kong must be greened to potentially cause a ~1 °C reduction. In addition, they found that the same could help improve daytime pedestrian thermal comfort by at least one thermal class, a higher greened façade ratio would be required to obtain similar thermal benefits in low- and medium-density urban settings, and benefits at pedestrians' height could be enhanced when vertical greenery facilities are placed at the podium rather than at the tower height. The layout size of building blocks ranged from 20 × 40 m² to 20 × 80 m² and 80 × 80 m², the street widths were 10, 15, 20, and 30 m, and the building block height was 60 m, which represented the realistic average building height in the selected area case. They concluded that 30–50% of façades in the high-density urban setting of Hong Kong must be greened to potentially cause a ~1 °C reduction, and the same could help improve daytime pedestrian thermal comfort by at least one thermal class. A higher greened façade ratio would be required to obtain similar thermal benefits in low- and medium-density urban settings, and

the benefits at pedestrian height could be enhanced when vertical greenery facilities are placed at the podium rather than at the tower height. In contrast with parametric scenario studies, more papers selected an urban morphology case or used a green wall module to study the performance of vertical greenery [36–38]. Tan C. et al.'s [36] research quantified the effect of MRT on outdoor thermal comfort from two green walls and indicated that the MRT was decreased significantly with vertical greenery both during the day and at night. Rupasinghe H. et al. [37] developed a series of vertical greenery systems (VGSs) to achieve maximum benefits on thermal performance in tropical Sri Lanka, which proved that living walls achieve better thermal performance with a record maximum temperature reduction of 10.16 °C, 3.31 °C, and 2.11 °C in the external wall surface, internal wall surface, and internal air temperature, respectively. As indicated above, research on actual site cases and green wall installations is often conducted using field measurements, while simulation methods are used for parametric studies more generally.

Previous studies also focused on the interacting mechanisms between VGS and FIPV. Specifically, Moren M., et al. [34] analyzed the influences of the 'Multifunctional System: Building Greening and Photovoltaic' (MFS) on the building façade temperature and further studied how the green buffer space impacts the temperature of PVs [34,39]. An east façade of wood material was divided into four parts, with the characteristics of function as a reference, including equipped with horizontal PV and greening, equipped with vertical PV and greening, and equipped with PV only, respectively. The façade temperature was measured yearly, monthly, daily, and hourly and analyzed to obtain a comprehensive overview of the system's performance under different weather conditions throughout the year. The above studies demonstrated that the façade temperature can benefit from MFS all year round, with average reductions from 21.4 °C to 30 °C for the maximum temperatures observed in the summer and habitations of heat loss on the façade up to 3 °C on average. In addition, the green buffer space reduced the PV operating temperature in the range of 1 °C–4 °C, and the benefits were the tendency to become higher under higher outdoor temperatures. Compared with the research of Moren M. et al. [34], other studies focused on façade renovation regarding FIPV and the vertical greening system. Wu Z. et al. [40] proposed the integration of a new solar photovoltaic collector with vertical green balconies in old high-rise buildings considering façade reconstruction concepts mainly focused on the water heating application for the purpose of rebuilding an old high-rise building. The reconstruction strategy considered the PVs' integration in the vertical green balconies where existing façades were replaced with PV façades, and the heat collector was combined with the building shading, which served as shade and a heat collector simultaneously. As for vertical greening, the balcony space was created to manage green plants. A CFD simulation using PHOENICS software was conducted to analyze annual energy-saving potential, thermal efficiency, and wind load, which would increase safety stress on surrounding skyscrapers. The study by Wu Z. et al. [40] indicated that PV collectors integrated with vertical green balconies are feasible. The simulation results of the design scheme showed that the integrated system offers benefits for ecology, e.g., purifying indoor air, regulating temperature and humidity indoors, inhaling carbon dioxide, and exhaling oxygen. Similar to Wu Z. et al. [40], Fluent was applied by Paskert et al. [41] to study airflow in a façade greening system equipped with photovoltaic modules. The system was horizontally distributed, with those farthest from the façade being the transparent PV modules followed by the plants and substrate containers, and the closet being the ventilation air gap. Then, based on the simulation results for the influence of surroundings with different roughness on airflow through the system, the air velocity of the greened and bare façade, the average air velocities and air change rates from the different simulated models, and the velocity within the façade greening modules were analyzed. The analyzed results indicated that the velocity of the greening system was lower than that of the bare façade. The study by Paskert et al. [41] inserted user-defined functions in the Fluent tool to simulate airflow around vertical greening and PVs, which is regarded as a creative

method, but heat transfer was not simulated, which is more important for vertical greening performance than airflow in general.

1.2.2. Review of Wind-Driven Rain

Until now, the existing research on WDR in building science has primarily focused on two aspects. One aspect involves quantifying WDR loads, while the other examines how buildings respond to these loads [25]. The research on WDR loads and their impact on building design typically relies on field measurements, semi-empirical estimations, and CFD simulation, with the latter being the dominant method [42,43]. Previous studies investigating building response to WDR loads have mainly concentrated on the effects of WDR impingement on building façades [44,45]. Several researchers have aimed to understand how WDR interacts with building components, such as façades, roofs, windows, and other exposed surfaces [24,46,47]. The goal is to assess the potential risks and consequences of WDR, including water infiltration, moisture damage, corrosion, and degradation of building materials [48,49]. Some studies of WDR involve analyzing its characteristics, such as droplet size, velocity, and trajectory, as well as the influence of wind speed, direction, and rain intensity. Researchers often use experimental techniques, numerical simulations, and field measurements to investigate WDR behavior and its effects on building performance [50–52]. The above literature indicates that the research on WDR aims to inform building design, construction practices, and the development of protective strategies or mitigation measures to enhance the durability and resilience of buildings against WDR. By understanding WDR patterns and their interaction with buildings, researchers seek to improve the overall performance and longevity of structures in various climatic conditions.

Furthermore, WDR also has an impact on UHI through greenery in urban spaces. Derome et al.'s [53] research indicated that the application of greening, e.g., green roofs, green façade, and urban gardens, on the surface of a building/urban district can potentially mitigate the UHI phenomenon and improve UMC because vegetation, e.g., grass, small plants, and trees, significantly influence the absorption, transport, and storage capacity of heat and moisture in the built environment. Well-built greening space is capable of promoting a heat decrease due to transpiration and evaporation [54]. However, numerical studies of UHI often simplify the sources of moisture and the coupling of moisture and heat transport occurring at the urban vegetation surface [53]. The impact of moisture transport within surfaces on the complex behavior of UHI is yet to be fully understood. WDR intensity must be considered as it is an important boundary condition in studies on the water cycle in the built environment, which can be a parameter of UHI, particularly when studying the cooling effect due to evaporation in the built environment.

1.3. Research Objectives

As indicated by the above literature, little has been studied regarding the application of VGSs at the urban district scale, synthesizing the climate-resilient potentials for both rainwater management and UHI mitigation. Therefore, this study explores this research gap, develops basic design strategies for VGSs in high-density built environments based on the WDR harvesting potential, and aims to assess the mitigation effect of VGSs with different coverage ratios on UHI. This study can provide references for architects and urban planners in planning a VGS at the urban district level in the early design stage.

Specifically, Part 1 introduces the research background and literature review regarding VGSs and WDR. Part 2 clarifies materials and methods mainly concerning the simulation of WDR and UHI. Part 3 analyzes the simulation data, while Part 4 summarizes this study and discusses future research directions as well as compares it with existing research. Finally, Part 5 draws some conclusions based on the simulation data and discussion.

2. Materials and Methods

The research objectives of this study include: (1) identifying the suitable façade locations for VGS application in existing high-density contexts of Hong Kong based on WDR

harvesting potential and (2) assessing the mitigation effect of VGSs with different coverage ratios on UHI in high-density, high-rise urban contexts.

This research combines quantitative analysis and qualitative study, a series of computational simulations, field investigation, and expert workshops. To provide a more realistic investigation scenario, the city of Hong Kong was taken as a case study. A 250 m by 250 m urban region in the Kowloon East district was selected as the analysis site.

To begin with, the urban morphology data were derived from the Hong Kong Lands Department [55] and open-source OpenStreetMap, and a 3D urban district model was generated in Grasshopper 7.13 software for further analysis. Two professional simulation software programs were applied: Ansys Fluent 2021R2 [56], for the wind-driven rain simulation, and ENVI-met V5.51 [57], for the VGS' UHI effect mitigation performance analysis.

Then, an interdisciplinary mini-design workshop was conducted after inviting architects, green building engineers, and landscape architects with expertise in greenery to join. Two architects, one urban designer, two landscape architects, and two green building engineers participated in this mini-design workshop lasting around 4 h. Three design proposals with different VGS coverage ratios were co-developed during this workshop (consisting of simulation data analysis, design brainstorming, and proposal development) for the next step in the analysis. In the low-coverage Scenario 1, only façade areas with very high WDR harvesting amounts were integrated with a VGS, while Scenario 2, with a moderate-coverage ratio, had a VGS on façade areas with moderate WDR harvesting areas. In Scenario 3, with a high coverage ratio, a VGS was applied to façade areas with large WDR harvesting areas.

In the last step, another workshop was conducted, and the potential challenges and corresponding strategies of applying VGSs in high-density urban contexts were discussed, with the synthesis of the simulation results.

2.1. Case Study of Urban Morphology

The parametric investigation was conducted using the Kowloon East district in Hong Kong as a case study, representing a typical urban morphology. This case has a high density and high plot ratio, which is characterized by a high average building height (Figure 3). In this case, the height of the tallest building is 92 m, and the buildings exhibit an irregular clustering arrangement. The reason for selecting this case is not only because it features high-density high-rise buildings, but also because the irregular urban morphology it presents brings about complex wind patterns and wind-driven rain distributions, which closely resemble real-world conditions.

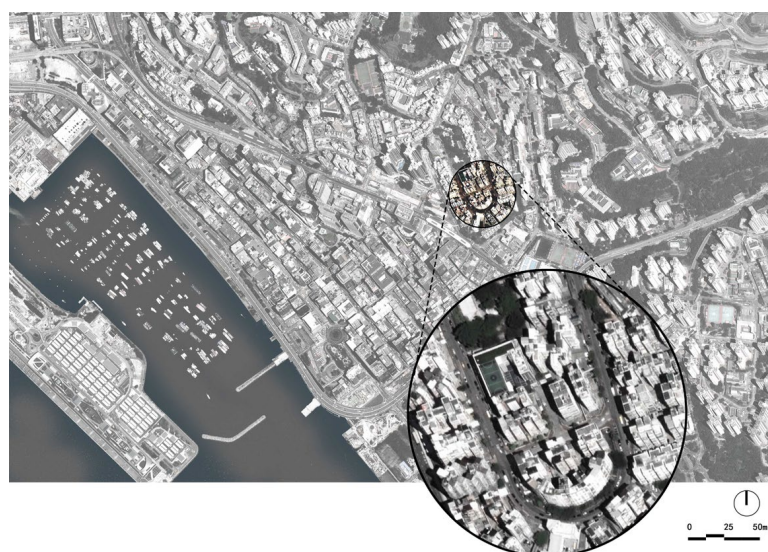


Figure 3. Overview of the selected case.

2.2. Wind-Driven Rain Simulation

2.2.1. Governing Equations of the Wind Phase

Before rain simulation, a 3D steady-state RANS method combined with a turbulence model of realizable $k-\epsilon$ was applied to capture the wind flow field in the commercial computational fluid dynamic (CFD) software Ansys Fluent 2021R2 [58]. In terms of incompressible flow, the equation governing the variables k and ϵ in a realizable $k-\epsilon$ turbulence model can be formulated as follows [59]:

$$\frac{\partial(\rho k)}{\partial t} + \frac{\partial(\rho k u_i)}{\partial x_i} = \frac{\partial}{\partial x_j} \left[\left(\mu + \frac{\mu_t}{\sigma_k} \right) \frac{\partial k}{\partial x_j} \right] + P_k + P_b - \rho \epsilon - Y_M + S_k \tag{1}$$

$$\frac{\partial(\rho \epsilon)}{\partial t} + \frac{\partial(\rho \epsilon u_i)}{\partial x_i} = \frac{\partial}{\partial x_j} \left[\left(\mu + \frac{\mu_t}{\sigma_\epsilon} \right) \frac{\partial \epsilon}{\partial x_j} \right] + \rho C_1 S_\epsilon - \rho C_2 \frac{\epsilon^2}{k + \sqrt{\nu \epsilon}} + C_{1\epsilon} \frac{\epsilon}{k} C_{3\epsilon} + S_\epsilon \tag{2}$$

where u_i represents the Cartesian components of the fluid velocity, ρ denotes the fluid density, k represents the turbulent kinetic energy, ϵ represents the turbulent energy dissipation rate, μ is the viscosity, and μ_t represents the turbulent viscosity. The term C_1 is determined as the maximum value between 0.43 and $\eta / (\eta + 5)$, where η is defined as S_k / ϵ . P_k and P_b represent the generation of turbulence kinetic energy due to average velocity gradients and buoyancy, respectively. The turbulent Prandtl numbers for k and ϵ are denoted as σ_k ($\sigma_k = 1.0$) and σ_ϵ ($\sigma_\epsilon = 1.2$) respectively. Additionally, the constants $C_{1\epsilon}$ ($C_{1\epsilon} = 1.44$) and C_2 ($C_2 = 1.9$) are included in the equation.

For wind simulation, the inlet boundary condition is specified using a Logarithmic Law profile, which can be expressed by the following equations:

$$U(z) = U_{10} \cdot K_r \cdot \ln\left(\frac{z}{z_o}\right) \tag{3}$$

where z represents the height coordinate, z_o is the roughness length, and U_{10} denotes the wind velocity at a height of 10 m.

The values of z_o and K_r are defined based on the terrain roughness category (in this paper, category B was considered). Related items and values can be found in Richards' paper [60].

2.2.2. Governing Equations of the Rain Phase

After the wind simulation, the Discrete Phase Model (DPM) coupled with the Eulerian Wall Film (EWF) model was used to simulate raindrop trajectories and film thickness. In the DPM, the trajectories of raindrops were calculated using the Lagrangian particle tracking method (LPT) in Lagrangian coordinates, which can be expressed by the following equation of raindrop motion:

$$\left(\frac{\rho_w - \rho}{\rho_w} \right) \vec{g} + \frac{3\mu}{\rho_w d^2} \frac{C_d R_{eR}}{4} \left(\frac{\vec{u}}{U} - \frac{d}{dt} \frac{\vec{r}}{r} \right) = \frac{d^2}{dt^2} \frac{\vec{r}}{r} \tag{4}$$

where ρ_w represents the density of the raindrops, ρ denotes the density of the air, g stands for the gravitational acceleration, d represents the diameter of a raindrop, μ symbolizes the dynamic viscosity of air, C_d represents the drag coefficient of a raindrop, $\frac{\vec{u}}{U}$ represents the mean velocity vector, \vec{r} signifies the position vector of the raindrop in the xyz-space, t denotes the time coordinate, and R_{eR} corresponds to the relative Reynolds number, which can be expressed as:

$$R_{eR} = \frac{\rho d}{\mu} \left\| \frac{\vec{u}}{U} - \frac{d}{dt} \frac{\vec{r}}{r} \right\| \tag{5}$$

During the simulation of raindrop trajectories using DPM, the EWF model was coupled with it to calculate rain films on the building façades. The conservation of mass in EWF is [61]:

$$\frac{\partial h \rho_f}{\partial t} + \nabla_s \cdot \left(\rho_f h \vec{v}_f \right) = \dot{m}_s \quad (6)$$

where h represents the film height, ∇_s denotes the surface gradient operator, \vec{v}_f represents the mean film velocity, \dot{m}_s represents the mass source per unit of wall surface, and ρ_f corresponds to the film density. The conservation of film momentum can be expressed as follows:

$$\frac{\partial h \vec{v}_f}{\partial t} + \nabla_s \cdot \left(h \vec{v}_f \vec{v}_f \right) = -\frac{h \nabla_s P_L}{\rho_f} + h \vec{g}_\tau + \frac{3}{2\rho_f} \vec{T}_{fs} - \frac{3V_f}{h} \vec{v}_f + \frac{\dot{q}}{\rho_f} \quad (7)$$

where P_L represents the water film pressure, \vec{g}_τ represents the gravity component normal to the surface, \vec{T}_{fs} represents the viscous shear force at the water–air interface, and \dot{q} denotes the momentum source term associated with raindrop interaction. The P_L can be calculated using Equations (8)–(10), where P_{gas} represents the gas pressure, ρ denotes the air density, \vec{n} represents the normal vector, \vec{g} represents the gravity vector, and σ corresponds to the surface tension.

$$P_L = P_{gas} + P_z + P_\sigma \quad (8)$$

$$P_z = -\rho h \left(\vec{n} \cdot \vec{g} \right) \quad (9)$$

$$P_\sigma = -\sigma \nabla_s \cdot \nabla_s h \quad (10)$$

Discrete raindrops hitting a face on the façade boundary are absorbed into the film; therefore, their mass and momentum are integrated to the source terms in Equations (6) and (7).

The mass source term can be expressed as follows:

$$\dot{m}_s = \dot{m}_p \quad (11)$$

where \dot{m}_p represents the flow rate of the particle stream impinging on the fac. The momentum source term can be expressed as follows:

$$\vec{q}_s = \dot{m}_p \cdot \left(\vec{v}_p - \vec{v}_f \right) \quad (12)$$

where \vec{v}_p is the velocity of the particle stream and \vec{v}_f is the film velocity.

2.2.3. Computational Domain and Boundary Conditions

In order to meet the criteria for the limits of distance to the domain, i.e., 5H to the sides and inlet, 6H to the top, and 15H to the outlet [62], the dimensions of the computational domain were set as 2190 m × 1170 m × 600 m, where H = 92 m is the height of the highest building (Figure 4).

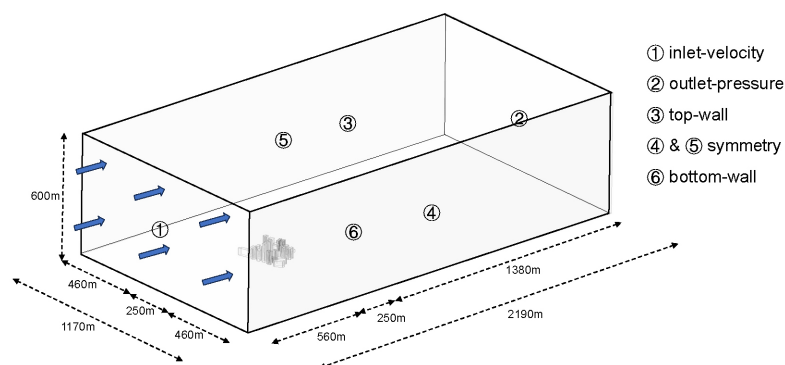


Figure 4. Computational domain.

In fact, the computational domain size was intentionally chosen to be larger than what would be necessary for the calculation. This ensured that the raindrops injected from an elevated position against the wind flow were not influenced by the presence of the building. As a result, the blockage ratio was determined to be 2.1%, which is lower than the recommended value of 3% based on previous research [62].

To calculate the boundary conditions of wind, U_{10} was defined as 5 m/s with an east direction, which represents the average wind speed and direction in the Kowloon East district. In the computational domain, wall conditions were applied to all boundaries except for the inlet and outlet. For pressure–velocity coupling, the coupled algorithm was utilized. The pressure interpolation was performed using a second-order scheme, and second-order discretization schemes were used for both the convection terms and the viscous terms of the governing equations.

Rainfall intensities (R_h) of 64, 100, and 200 mm/h which represent the different degrees of extreme rain events, were selected to determine the raindrop diameter using simulation. A raindrop diameter of 2.5 mm, which represents the highest density probability of 64 and 100 mm/h, while a higher of 200 mm/h was selected (Figure 5) according to Best et al.’s research concerning the probability density of raindrop size [63]. The initial horizontal velocity of a raindrop was equal to the wind velocity, while the initial vertical velocity was calculated from Blocken et al.’s measurements [64]. The raindrops were released at a height of 500 m to allow sufficient time for them to attain their steady terminal velocities before entering the airflow field, which was perturbed by the presence of the target buildings. The injection type was group, and each group had 10,000 streams. The groups were located on the top surface of the computational domain, with a spacing of 10 m between each group until the entire top surface was filled.

2.3. Simulation of the Impact of VGS on UHI

2.3.1. ENVI-Met Theory

Based on the Ansys Fluent simulation results, the urban façade areas were categorized into 5 levels of wind-driven rain occurrence potentials: very high, high, moderate, low, and very low. Vertical greenery was implemented at locations where there was a very high, high, and moderate likelihood of occurrence potential on the façades, and then the impact of vertical greenery on the UHI effect was simulated using ENVI-met V5.5.1 [65]. ENVI-met is a CFD model that utilizes the Reynolds-Averaged Navier–Stokes (RANS) equations integrated with the standard $k-\epsilon$ turbulence model [66]. The outstanding advantage of ENVI-met is that plants are living organisms that actively interact with their surrounding environment through energy absorption and evapotranspiration processes. Façade greenery can be appended on the grid of the external façade to provide shading from direct sunlight, and plants can effectively cool the surface of walls, decrease the emission of longwave radiation, and change the overall thermal environment [67]. Note that the reduced temperature ($\Delta T = T_{bare\,façade} - T_{green\,façade}$) in street canyon was applied as the evaluation index for the mitigation effect of a VGS on UHI.

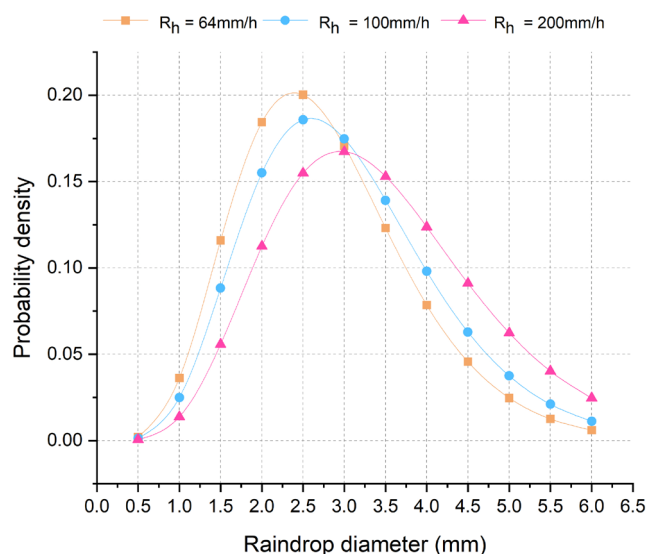


Figure 5. Probability distribution of raindrop size for a rainfall intensity of 64 mm/h.

2.3.2. ENVI-Met Simulation Setup

The 3D model with façade greenery was constructed in the “ENVI-met space” module, and the domain size was 430 m × 430 m × 290 m with grids in the x -axis, y -axis, z -axis directions of 3 m, 3 m, and 3 m, respectively. The façade greenery was set as “only greenery”, which was not considered a substance. Materials for the façade, roof, and pavement were set as glass bricks, a concrete wall, and a dark concrete pavement, respectively. The hourly temperature and relative humidity for July 1st of a Typical Meteorological Year (TMY) were used as boundary conditions for the “Simple Force” methodology. On this particular day, the minimum temperature recorded was 27 °C, and the maximum temperature reached 32 °C. The relative humidity ranged from 71% to 94%, while wind velocity was 2 m/s, in order to minimize the impact of heat convection. The simulation was conducted assuming a cloud-free sky condition to represent a sunny summer day for a duration of 24 h, from 6:00 to 5:59. Temperature data of 2 receptors located in different positions of the case for 6:00 to 5:59 were used in order to calculate compare temperature difference (Table 1). Ivy plants, i.e., *Hedera helix*, were selected as the façade greenery, which has been known to have a cooling effect on a surrounding area, making them a popular choice for landscaping and façade greening purposes [68].

Table 1. Parameter settings in ENVI-met.

Category	Set Detail
Methodology	Simple forcing
Maximum temperature	32 °C
Minimum temperature	27 °C
Maximum humidity	94%
Minimum humidity	71%
Wind speed	2 m/s
Wind direction	90 °C at inflow
Grid size	1 m
Grid amount of x -axis	430
Grid amount of y -axis	430
Grid amount of z -axis	290
Greenery type	Green + sandy loam substrate
Façade material	Glass bricks
Roof material	Concrete wall
Pavement material	Concrete pavement dark

Table 1. Cont.

Category	Set Detail
Leaf area index	1.5
Leaf angle distribution	0.5
Emissivity of substrate	0.95
Albedo of substrate	0.3
Water coefficient of substrate for plant	0.5
Air gap between substrate and wall	0.01 m
Greenery species	Hedera helix

The UHI mitigation effects of three different design proposals were simulated and analyzed by comparing the temperature of receptors and street canyon using temperature data and temperature color (Figure 6). The original urban morphology model without a VGS was also simulated to provide a reference.

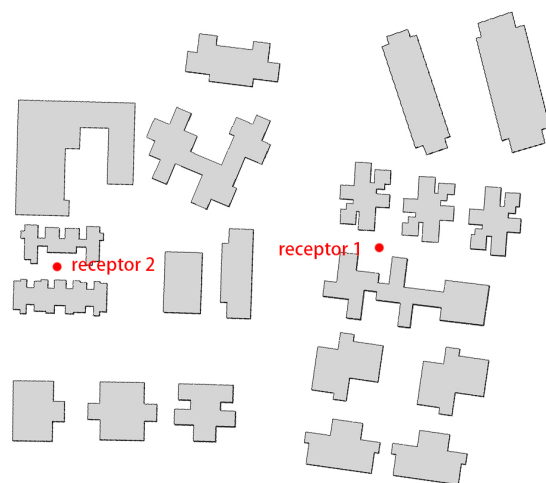


Figure 6. Location of receptors.

3. Results

3.1. Wind-Driven Rain Simulation Results

The most potential distribution of WDR occurs on the roof, as there is no obstruction on the roof. In terms of building façades, the windward façade is heavily affected by WDR compared with other façades, and the façade near the roof is most subject to WDR. The trajectory of raindrops visually reflects the areas on the façade that are prone to being wetted by WDR (Figure 7). In addition to the roof, the lower part of the building façade is another area prone to water accumulation. Implementing VGS in this area has two advantages: firstly, it reduces maintenance costs, and secondly, the collected rainwater can be used as natural irrigation for the green plants, thus sustaining their growth. The areas with the highest amount of WDR are primarily located at the bottom of the façade and near the roof. Additionally, building façades without obstructions on the periphery receive more WDR. The façades on the interior, due to the shielding effect of adjacent buildings, experience a significant decrease in the distribution area and thickness of the rain film caused by WDR. Based on the distribution of rain film thickness caused by WDR on building façades, this study categorizes the occurrence potential of WDR into five levels, i.e., very high, high, moderate, low, and very low. The proportions of each level on the façade were also calculated to provide a more accurate assessment of the distribution of WDR on the façades.

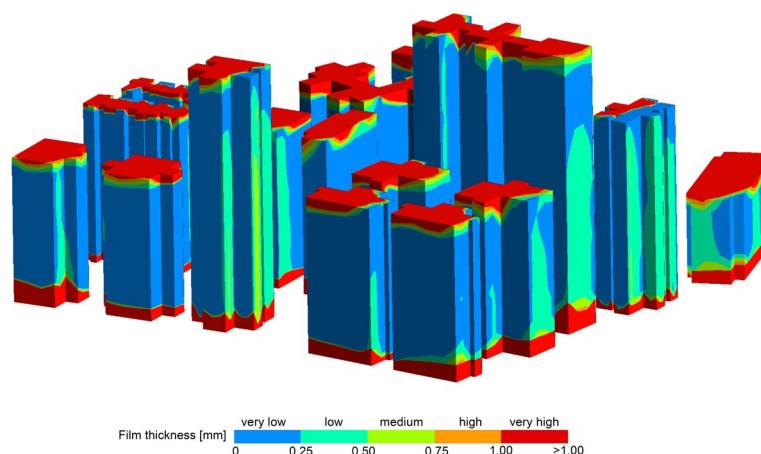


Figure 7. Wind-driven rain distribution on building façades.

As indicated by the color blocks, the areas on the façade where WDR occurs can be visually matched with a VGS. Three proposals can be extracted accordingly: a VGS is only implemented in areas with very high (Scenario 1), very high and high (Scenario 2), and very high, high, and moderate (Scenario 3) WDR-harvesting potential (Figure 8). The average coverage ratios of Scenarios 1, 2, and 3 are 17%, 21%, and 22%, respectively. For each building façade in the case study, VGSs were conducted following the same approach. The simulation results of the well-handled model in ENVI-met can be found in Section 3.2.

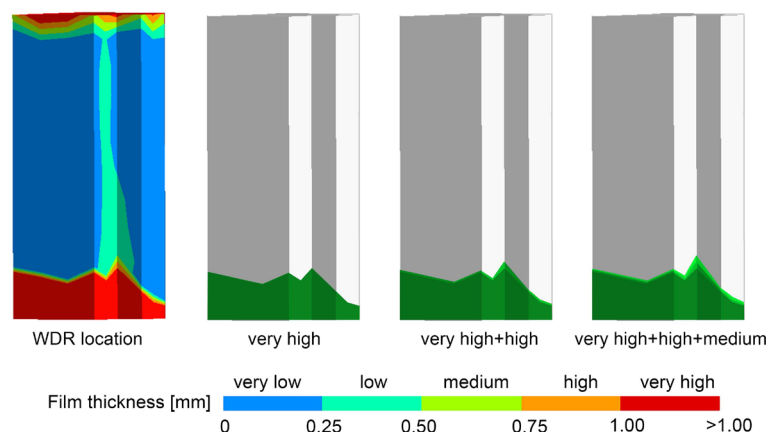


Figure 8. Vertical greenery coverage according to WDR distribution.

3.2. UHI Mitigation Simulation Result

3.2.1. Pedestrian Temperature Distribution

The data from both measurement points indicate that within a 24-h period, the highest temperature occurs at 1 p.m., with values of 32.57 °C and 32.81 °C, respectively, and the temperatures at 12 p.m. and 2 p.m. are slightly lower than at 1 p.m. During the night and early morning, the temperature reaches its lowest point, around 27 °C. However, vertical greenery has minimal cooling effect during the night, which could be due to the fact that green plants are unable to undergo the process of evapotranspiration during the evening hours. Despite the same VGS design, the cooling effect at receptor 1 is better than at receptor 2. This difference may be attributed to variations in urban morphology and building forms. Further, compared with the bare scenario, the application of the VGS leads to a noticeable reduction in temperature differences at the pedestrian height level. However, as the VGS coverage ratio increases, the temperature differences become less significant. This indicates that placing greenery in the lower parts of the façades is more beneficial for mitigating the UHI effect at pedestrian height. There are several reasons why temperature differences may not be significant despite an increase in the greenery coverage

ratio: As the VGS coverage ratio increases, the cooling effect provided by the greenery reaches a saturation state, which means the cooling effect does not significantly change. In addition, changes in temperature differences may be influenced by other factors such as building morphology [69], the surrounding environment [70], and climate conditions [71]. These factors can mask the impact of an increased greenery coverage ratio on temperature differences. The cooling effect of plants becomes significant starting at 7 a.m. in the morning, while from 3 p.m. onward, the temperature difference gradually decreases, and during the night, the temperature difference is minimal. The maximum temperature difference is reached between 12 p.m. and 2 p.m. during the day (Figure 9).

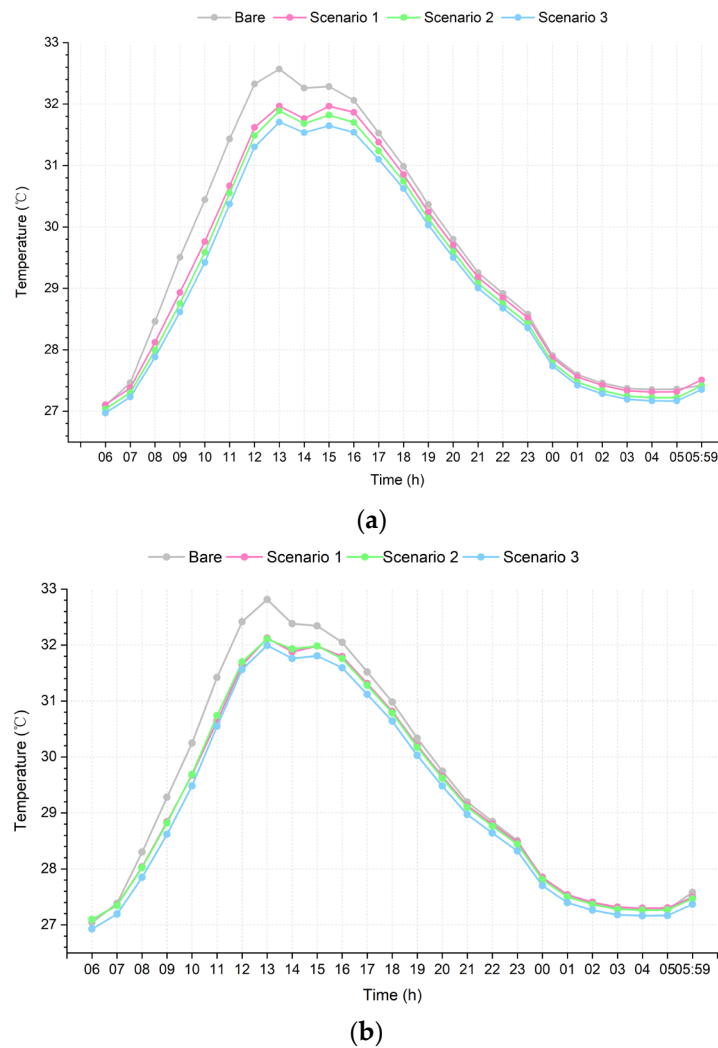
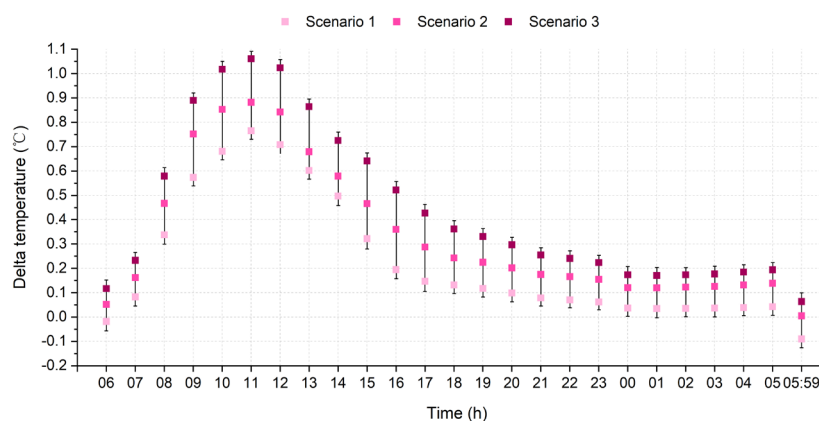


Figure 9. The temperature at every moment within 24 h: (a) receptor 1 and (b) receptor 2.

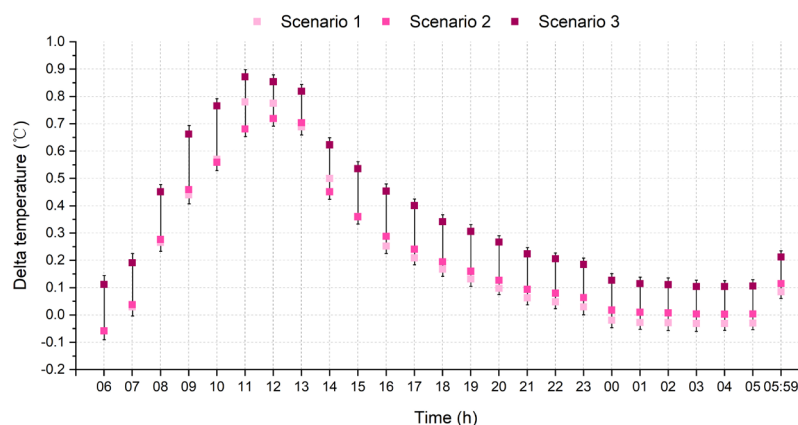
3.2.2. Pedestrian Temperature Reduction with a VGS

It can be observed from Figure 10 that at receptor 1, vertical greening achieves relatively ideal cooling effects on the UHI between 9 a.m. and 2 a.m. At receptor 2, the cooling effect is relatively ideal during the period from 10 a.m. to 1 p.m. The best cooling effect at receptor 1 is observed at 11 a.m., with temperature reductions of 0.76 °C, 0.88 °C, and 1.06 °C for Scenario 1, Scenario 2, and Scenario 3, respectively. At receptor 2, Scenario 3 achieves the best cooling effect at 11 a.m., with a temperature decrease of 0.87 °C. Scenario 1 shows the best cooling effect at 12 p.m., with a temperature difference of 0.78 °C, while Scenario 2 achieves the best cooling effect at 12 p.m., with a temperature decrease of 0.71 °C. As the VGS coverage ratio increases, there is a significant increase in temperature difference at receptor 1, indicating a notable improvement in alleviating the UHI effect. However, the

temperature difference at receptor 2 remains relatively unchanged. This could be due to the orientation of the façades near receptor 2, which face west or north. The cooling effect of vegetation in these directions may naturally be less significant compared with the south and east directions. In addition to the façade orientation, there are other potential factors that could contribute to the minor temperature difference at receptor 2: If the façades at receptor 2 are directly exposed to sunlight, it can increase surface temperatures and reduce the cooling effect of vertical greening. In addition, the direction and speed of winds can influence the temperature at receptor 2. Higher wind speeds may diminish the cooling effect provided by the VGS. And the urban morphology can also impact the temperature difference at receptor 2. High-density buildings can contribute to a more intensive UHI effect, resulting in a relatively smaller cooling effect from a VGS.



(a)



(b)

Figure 10. The absolute temperature difference at every moment within 24 h: (a) receptor 1 and (b) receptor 2.

4. Discussion

The aim of this study is to explore the mitigation effect of façade-integrated vertical greening on the UHI phenomenon in the high-density city of Hong Kong, particularly on high-rise building façades with the consideration of WDR. Considering the natural irrigation provided by WDR, which enhances plant transpiration and evaporation, and its potential to alleviate the UHI effect, the VGS was strategically placed in areas with higher WDR levels. Based on the distribution of WDR on the building façades, three VGS design schemes were proposed: (1) Vertical greening is only implemented at positions with a very high WDR amount on the façades; (2) vertical greening is implemented at very high and high positions on the façades; and (3) vertical greening is implemented

at very high, high, and moderate positions on the façades. In ENVI-met, simulations were conducted to analyze the microclimate effects of the three VGS design schemes compared to the original case study model without any greenery. Existing studies have focused on either the mitigating effects of vertical greenery on UHI or the impact of WDR on buildings [72,73] without studying the combination of both factors. This study first integrated WDR with a VGS, i.e., determined the location of a VGS based on the façade's WDR-harvesting potential, which is the novelty of this research. The results indicate that the presence of vertical greenery can reduce temperatures within street canyons to a certain extent, and the cooling effect becomes more pronounced as the coverage ratio of the VGS increases. WDR has a significant impact on the UHI of cities, primarily through the processes of evaporation and transpiration of vegetation and water storage in the plant substrate. The façade-integrated vertical greenery design method based on WDR distribution proposed in this study, along with the assessment method for its mitigation effect on the UHI phenomenon, can provide a foundation for the design of vertical greenery. This method offers valuable guidance for incorporating WDR patterns into the planning and implementation of vertical greenery projects, thus contributing to the overall effectiveness and success of UHI mitigation strategies.

The limitations of this study include the following points: (1) Due to limitations imposed by ENVI-met software, the configuration of the VGS could not be fully aligned with the simulated results of WDR. It only provided a rough reference to the simulation results of WDR. (2) As the main objective of this study was to explore the mitigating effects of VGS on UHI under certain urban morphologies, details such as window-to-wall ratios and other architectural façade elements were not taken into account. (3) Due to limitations of the simulation software, the impact of rainfall on temperature and humidity was not considered. Considering these impacts would enable a more accurate simulation of the effects of VGSs on UHI.

Although a large number of researchers have emphasized the cooling effect of VGSs on UHI or the WDR's impact on building façades [72,73], no study has integrated WDR, VGSs, and UHI, which involves determining the VGS's location on a façade based on WDR-harvesting potential for its irrigation benefit and then assessing the mitigation effect of the VGS on UHI. In terms of receptor 1 in this study, a VGS could result in temperature-reduced ranges from 0 °C to 0.76 °C, 0 °C to 0.88 °C, and 0.07 °C to 1.06 °C for Scenario 1 (17% coverage ratio), Scenario 2 (21% coverage ratio), and Scenario 3 (22% coverage ratio), respectively. However, the results presented in this study show a higher temperature decrease compared with the findings of another simulation study conducted by Peng [74], in which a maximum cooling intensity of 0.96 °C was observed in a high-rise, high-density site. Furthermore, another simulation study [75] conducted in a similar climate in Singapore showed that a 100% green façade coverage of buildings in an estate resulted in a maximum temperature reduction of 1 °C. These variations can be attributed to differences in model physics, model configuration, thermal properties of building materials, and the representation of plants in their models compared with the ones used in our study. In addition, as the VGS coverage ratio increases, i.e., as the elevation of VGS increases, the cooling effect on UHI becomes less significant. This indicates that the vegetation located near the pedestrian level at the bottom of the façade has the greatest cooling effect on the street. This finding is consistent with early research conducted by Peng et al. [74] and Morakinyo et al. [35].

Indeed, research on WDR, VGSs, and the UHI effect is still in its early stages, and there are many fields that can be further explored in future studies. For example, integrating the solar energy harvest potential into the holistic design of VGS design and planning in urban contexts. The focus includes: (1) determining the optimal positions for FIPV panels and a VGS to maximize solar energy utilization and provide suitable growing conditions for plants and (2) the VGS should be able to withstand the weight of plants and WDR loads, while the FIPV should match the materials, structure, and color aesthetic of the building envelope. Combining building-integrated photovoltaics (BIPV) with VGSs can be a win-win solution since the evaporation effects of VGSs could enhance the PV performance by

cooling the system's operation temperature [76]. Integrating water resources is another emphasis for the future because it can help alleviate the urban drainage burden caused by extreme typhoons and heavy rainfall. In the VGS design, considering the collection and utilization of WDR for plant irrigation can reduce reliance on the urban water supply system and increase the sustainability of the system. Calculating the impact of integrated VGS and FIPV systems on urban microclimates, building energy consumption, and carbon emissions is also an important field of future research. Specifically, the effects of VGS and PV integrated systems on urban microclimate parameters such as temperature, humidity, and wind patterns and quantifying the extent to which the systems can mitigate the UHI effect and improve urban microclimate. It is also important to assess the energy performance of buildings with integrated VGS and PV systems; analyze their impact on building energy consumption, including reductions in cooling and heating loads; evaluate the potential for energy generation using photovoltaic panels; and calculate the carbon emission reductions achieved with integrated systems. Finally, we should consider the lifecycle assessment of materials used in vertical greenery and photovoltaic systems, as well as the carbon sequestration potential of plants, and assess the overall carbon footprint of the integrated systems and compare it with conventional building systems. It is also worth noting that not all vertical green technological solutions are applicable to high-rise buildings due to wind and structural considerations, sunlight and shading, maintenance and accessibility, and space constraints.

5. Conclusions

This study proposes three VGS design schemes based on the WDR quantity and distribution on building façades. The mitigation effects of these three schemes on the UHI phenomenon were compared, and the following conclusions were drawn:

- (a) In high-density, high-rise building clusters, the WDR amounts are highest on the façades near the roof and at the bottom of the façades without obstructions on the periphery. It gradually decreases from the ends of the façades toward the middle. This distribution pattern is likely influenced by wind patterns and the blocking effect of neighboring buildings.
- (b) The maximum temperature difference on the street occurs between 12 PM and 3 PM, indicating the greatest mitigation of the UHI effect. Scenario 1, Scenario 2, and Scenario 3 achieve maximum temperature differences of 0.76 °C, 0.88 °C, and 1.06 °C, respectively, during this time period.
- (c) VGSs can indeed mitigate the UHI effect in high-density urban contexts with high-rise buildings. Furthermore, there is a general trend of improved mitigation as the VGS coverage ratio increases. However, it is important to note that the extent of UHI mitigation is the result of multiple factors working together, and it does not necessarily exhibit a linear relationship with the coverage ratio of a VGS.

The proposed VGS design method for high-density, high-rise building façades based on WDR position and its evaluation method for mitigating the UHI effect provides a theoretical basis for utilizing WDR at an urban scale and mitigating the Urban Heat Island effect. However, when it comes to actual design implementation, it is necessary to consider the comprehensive effect of multiple factors and seek a trade-off.

Author Contributions: Conceptualization, C.X.; methodology, C.X.; software, L.T. and C.X.; writing—original draft preparation, C.X.; writing—review and editing, C.X. and L.T. All authors have read and agreed to the published version of the manuscript.

Funding: This study was sponsored by the research startup fund R9832 at the Hong Kong University of Science and Technology (HKUST). The authors express sincere gratitude to the HKUST and the Hong Kong University Grants Committee.

Data Availability Statement: The data presented in this study are available on request from the corresponding author. The data are not publicly available due to sharing limitations of document format of illustration software.

Conflicts of Interest: The authors declare no conflict of interest.

References

1. Mirza, M.M.Q. Climate Change and Extreme Weather Events: Can Developing Countries Adapt? *Clim. Policy* **2003**, *3*, 233–248. [CrossRef]
2. Frame, D.J.; Rosier, S.M.; Noy, I.; Harrington, L.J.; Carey-Smith, T.; Sparrow, S.N.; Stone, D.A. Dean Climate Change Attribution and the Economic Costs of Extreme Weather Events: A Study on Damages from Extreme Rainfall and Drought. *Clim. Chang.* **2020**, *162*, 781–797. [CrossRef]
3. Sajjad, M.; Chan, J.C.L. Tropical Cyclone Impacts on Cities: A Case of Hong Kong. *Front. Built Environ.* **2020**, *6*, 575534. [CrossRef]
4. Hong Kong Observatory Climate Change in Hong Kong—Extreme Weather Events | Hong Kong Observatory (HKO). Available online: https://www.hko.gov.hk/en/climate_change/obs_hk_extreme_weather.htm (accessed on 8 October 2023).
5. HKSAR A September with Super Typhoon Saola and Record-Breaking Rainstorm. Available online: <https://www.info.gov.hk/gia/general/202310/04/P2023100300488.htm> (accessed on 9 October 2023).
6. Environment Bureau. *Hong Kong's Climate Action Plan 2030+*; Environment Bureau: Hong Kong, China, 2017.
7. He, J.; Qiang, Y.; Luo, H.; Zhou, S.; Zhang, L. A Stress Test of Urban System Flooding upon Extreme Rainstorms in Hong Kong. *J. Hydrol.* **2021**, *597*, 125713. [CrossRef]
8. UN News Hottest July Ever Signals 'Era of Global Boiling Has Arrived' Says UN Chief. Available online: <https://news.un.org/en/story/2023/07/1139162> (accessed on 8 October 2023).
9. Givoni, B. *Climate Considerations in Building and Urban Design*; John Wiley & Sons: New York, NY, USA, 1998; ISBN 978-0-471-29177-0.
10. Hui, S.C.M. Low Energy Building Design in High Density Urban Cities. *Renew. Energy* **2001**, *24*, 627–640. [CrossRef]
11. *Urban Climatic Map and Standards for Wind Environment-Feasibility Study*; Planning Department, Hong Kong Government: Hong Kong, China, 2012.
12. Lai, E.T.C.; Chau, P.H.; Cheung, K.; Kwan, M.; Lau, K.; Woo, J. Perception of Extreme Hot Weather and the Corresponding Adaptations among Older Adults and Service Providers—A Qualitative Study in Hong Kong. *Front. Public Health* **2023**, *11*, 1056800. [CrossRef] [PubMed]
13. Hua, J.; Ren, C.; Shi, Y.; Lau, K.K.L.; Ng, E.Y.Y. Impact of Urban Overheating and Heat-Related Mortality in Hong Kong. In *Urban Overheating: Heat Mitigation and the Impact on Health*; Springer: Singapore, 2022; pp. 275–292. [CrossRef]
14. Ballester, J.; Quijal-Zamorano, M.; Méndez Turrubiates, R.F.; Pegenaute, F.; Herrmann, F.R.; Robine, J.M.; Basagaña, X.; Tonne, C.; Antó, J.M.; Achebak, H. Heat-Related Mortality in Europe during the Summer of 2022. *Nat. Med.* **2023**, *29*, 1857–1866. [CrossRef]
15. South China Morning Post Hong Kong's Hottest Summer Ever—Why Temperatures Keep Rising. Available online: <https://multimedia.scmp.com/infographics/news/hong-kong/article/3234514/urban-heat-island/index.html> (accessed on 8 October 2023).
16. Hong Kong Observatory Number of Very Hot Days. Available online: https://www.hko.gov.hk/en/cis/statistic/vhotday_statistic.htm (accessed on 8 October 2023).
17. Morakinyo, T.E.; Ren, C.; Shi, Y.; Lau, K.K.L.; Tong, H.W.; Choy, C.W.; Ng, E. Estimates of the Impact of Extreme Heat Events on Cooling Energy Demand in Hong Kong. *Renew. Energy* **2019**, *142*, 73–84. [CrossRef]
18. Fung, W.Y.; Lam, K.S.; Hung, W.T.; Pang, S.W.; Lee, Y.L. Impact of Urban Temperature on Energy Consumption of Hong Kong. *Energy* **2006**, *31*, 2623–2637. [CrossRef]
19. McFarland, A.R.; Larsen, L.; Yeshitela, K.; Engida, A.N.; Love, N.G. Guide for Using Green Infrastructure in Urban Environments for Stormwater Management. *Environ. Sci.* **2019**, *5*, 643–659. [CrossRef]
20. Zheng, X.; Zou, Y.; Lounsbury, A.W.; Wang, C.; Wang, R. Green Roofs for Stormwater Runoff Retention: A Global Quantitative Synthesis of the Performance. *Resour. Conserv. Recycl.* **2021**, *170*, 105577. [CrossRef]
21. Drainage Services Department. Sponge City: Adapting to Climate Change. Available online: https://www.dsd.gov.hk/Documents/SustainabilityReports/1617/en/sponge_city.html (accessed on 8 October 2023).
22. van de Wouw, P.M.F.; Ros, E.J.M.; Brouwers, H.J.H. Precipitation Collection and Evapo(Transpi)Ration of Living Wall Systems: A Comparative Study between a Panel System and a Planter Box System. *Build. Environ.* **2017**, *126*, 221–237. [CrossRef]
23. Gao, G.; Zhao, L.; Wang, C.; Grunewald, J. Lili Wind-Driven Rain on a Building Façade in Urban Environment. *Procedia Eng.* **2017**, *205*, 1678–1684. [CrossRef]
24. Gholamalipour, P.; Ge, H.; Stathopoulos, T. Wind-Driven Rain (WDR) Loading on Building Facades: A State-of-the-Art Review. *Build. Environ.* **2022**, *221*, 109314. [CrossRef]
25. Blocken, B.; Carmeliet, J. A Review of Wind-Driven Rain Research in Building Science. *J. Wind. Eng. Ind. Aerodyn.* **2004**, *92*, 1079–1130. [CrossRef]
26. Blocken, B.; Derome, D.; Carmeliet, J. Rainwater Runoff from Building Facades: A Review. *Build. Environ.* **2013**, *60*, 339–361. [CrossRef]
27. Jim, C.Y. Assessing Climate-Adaptation Effect of Extensive Tropical Green Roofs in Cities. *Landsc. Urban Plan.* **2015**, *138*, 54–70. [CrossRef]
28. Susca, T.; Zanghirella, F.; Colasuonno, L.; Del Fatto, V. Effect of Green Wall Installation on Urban Heat Island and Building Energy Use: A Climate-Informed Systematic Literature Review. *Renew. Sustain. Energy Rev.* **2022**, *159*, 112100. [CrossRef]
29. Mitterboeck, M.; Korjenic, A. Analysis for Improving the Passive Cooling of Building's Surroundings through the Creation of Green Spaces in the Urban Built-up Area. *Energy Build.* **2017**, *148*, 166–181. [CrossRef]

30. Vuckovic, M.; Kiesel, K.; Mahdavi, A. Studies in the Assessment of Vegetation Impact in the Urban Context. *Energy Build.* **2017**, *145*, 331–341. [[CrossRef](#)]
31. Anguluri, R.; Narayanan, P. Role of Green Space in Urban Planning: Outlook towards Smart Cities. *Urban For. Urban Green.* **2017**, *25*, 58–65. [[CrossRef](#)]
32. Khoshtaria, T.K.; Chachava, N.T. The Planning of Urban Green Areas and Its Protective Importance in Resort Cities (Case of Georgian Resorts). *Ann. Agrar. Sci.* **2017**, *15*, 217–223. [[CrossRef](#)]
33. Duarte, D.H.S.; Shinzato, P.; Gusson, C.d.S.; Alves, C.A. The Impact of Vegetation on Urban Microclimate to Counterbalance Built Density in a Subtropical Changing Climate. *Urban Clim.* **2015**, *14*, 224–239. [[CrossRef](#)]
34. Penaranda Moren, M.S.; Korjenic, A. Hotter and Colder—How Do Photovoltaics and Greening Impact Exterior Facade Temperatures: The Synergies of a Multifunctional System. *Energy Build.* **2017**, *147*, 123–141. [[CrossRef](#)]
35. Morakinyo, T.E.; Lai, A.; Lau, K.K.-L.; Ng, E. Thermal Benefits of Vertical Greening in a High-Density City: Case Study of Hong Kong. *Urban For. Urban Green.* **2019**, *37*, 42–55. [[CrossRef](#)]
36. Tan, C.L.; Wong, N.H.; Jusuf, S.K. Effects of Vertical Greenery on Mean Radiant Temperature in the Tropical Urban Environment. *Landsc. Urban Plan.* **2014**, *127*, 52–64. [[CrossRef](#)]
37. Rupasinghe, H.T.; Halwatura, R.U. Benefits of Implementing Vertical Greening in Tropical Climates. *Urban For. Urban Green.* **2020**, *53*, 126708. [[CrossRef](#)]
38. Malys, L.; Musy, M.; Inard, C. A Hydrothermal Model to Assess the Impact of Green Walls on Urban Microclimate and Building Energy Consumption. *Build. Environ.* **2014**, *73*, 187–197. [[CrossRef](#)]
39. Moren, M.S.P.; Korjenic, A. Green Buffer Space Influences on the Temperature of Photovoltaic Modules. *Energy Build.* **2017**, *146*, 364–382. [[CrossRef](#)]
40. Wu, Z.; Chul-Soo, K. A Preliminary Study Understanding the Possibility and Benefits of Solar Photovoltaic Collector Integration with Vertical Green Balconies in Building Facade Reconstruction. *Front. Energy Res.* **2023**, *10*, 1025564. [[CrossRef](#)]
41. Paskert, T.; Alsaad, H.; Voelker, C. Airflow through a Facade Greening System Equipped with Vertical Photovoltaic Modules. In Proceedings of the BauSim Conference 2022, Weimar, Germany, 20 September 2022.
42. Liu, M.; Li, Q.S.; Huang, S.H. Large Eddy Simulation of Wind-Driven Rain Effects on a Large Span Retractable Roof Stadium. *J. Wind. Eng. Ind. Aerodyn.* **2019**, *195*, 104009. [[CrossRef](#)]
43. Cho, E.; Yoo, C.; Kang, M.; Song, S.; Kim, S. Experiment of Wind-Driven-Rain Measurement on Building Walls and Its in-Situ Validation. *Build. Environ.* **2020**, *185*, 107269. [[CrossRef](#)]
44. Blocken, B.; Carmeliet, J. The Influence of the Wind-Blocking Effect by a Building on Its Wind-Driven Rain Exposure. *J. Wind. Eng. Ind. Aerodyn.* **2006**, *94*, 101–127. [[CrossRef](#)]
45. Blocken, B.; Carmeliet, J. On the Accuracy of Wind-Driven Rain Measurements on Buildings. *Build. Environ.* **2006**, *41*, 1798–1810. [[CrossRef](#)]
46. Dukhan, T.; Sushama, L. Understanding and Modelling Future Wind-Driven Rain Loads on Building Envelopes for Canada. *Build. Environ.* **2021**, *196*, 107800. [[CrossRef](#)]
47. Ferrari, A.; Kubilay, A.; Derome, D.; Carmeliet, J. The Use of Permeable and Reflective Pavements as a Potential Strategy for Urban Heat Island Mitigation. *Urban Clim.* **2020**, *31*, 100534. [[CrossRef](#)]
48. Chen, C.; Zhang, H.; Feng, C.; Xuan, Y.; Qian, T.; Xie, J. Analysis of Wind-Driven Rain Characteristics Acting on Building Surfaces in Shanghai Based on Long-Term Measurements. *J. Build. Eng.* **2022**, *45*, 103572. [[CrossRef](#)]
49. Vutukuru, K.S.; Moravej, M.; Elawady, A.; Chowdhury, A.G. Holistic Testing to Determine Quantitative Wind-Driven Rain Intrusion for Shuttered and Impact Resistant Windows. *J. Wind. Eng. Ind. Aerodyn.* **2020**, *206*, 104359. [[CrossRef](#)]
50. Xu, G.; Tan, K.; Ge, Z.; Poh, H.J.; Ooi, C.C.; Eng, Y. Automatic Selection of Release Plane for Lagrangian-Based Wind-Driven Rain Studies. *J. Wind. Eng. Ind. Aerodyn.* **2023**, *232*, 105242. [[CrossRef](#)]
51. Cacciotti, R. Brick Masonry Response to Wind Driven Rain. *Eng. Struct.* **2020**, *204*, 110080. [[CrossRef](#)]
52. Lu, B.; Fang, J.; Li, Y.; Zhang, H.; Gao, Y.; Feng, C. Accuracy of Semi-Empirical Models for Wind-Driven Rain Using Different Data Processing Methods for Wind Velocity and Direction. *Build. Environ.* **2023**, *237*, 110300. [[CrossRef](#)]
53. Derome, D.; Kubilay, A.; Defraeye, T.; Blocken, B.; Carmeliet, J. Ten Questions Concerning Modeling of Wind-Driven Rain in the Built Environment. *Build. Environ.* **2017**, *114*, 495–506. [[CrossRef](#)]
54. He, B.-J. Potentials of Meteorological Characteristics and Synoptic Conditions to Mitigate Urban Heat Island Effects. *Urban Clim.* **2018**, *24*, 26–33. [[CrossRef](#)]
55. Lands Department. 3D Mapping. Available online: <https://www.landsd.gov.hk/en/survey-mapping/mapping/3d-mapping.html> (accessed on 9 October 2023).
56. ANSYS. Ansys Fluent. Available online: <https://www.ansys.com/products/fluids/ansys-fluent> (accessed on 9 October 2023).
57. ENVI-met. GmbH ENVI-Met. Available online: <https://www.envi-met.com/> (accessed on 9 October 2023).
58. Zhan, J.-M.; Fan, Q.; Hu, W.-Q.; Gong, Y.-J. Hybrid $k - \epsilon$ /Laminar Method in the Application of 3D Heaving OWCs. *Renew. Energy* **2020**, *155*, 691–702. [[CrossRef](#)]
59. Qu, S.; Liu, S.; Ong, M.C. An Evaluation of Different RANS Turbulence Models for Simulating Breaking Waves Past a Vertical Cylinder. *Ocean. Eng.* **2021**, *234*, 109195. [[CrossRef](#)]
60. Richards, P.J.; Norris, S.E. Appropriate Boundary Conditions for Computational Wind Engineering Models Revisited. *J. Wind. Eng. Ind. Aerodyn.* **2011**, *99*, 257–266. [[CrossRef](#)]

61. Gunn, R.; Kinzer, G.D. The terminal velocity of fall for water droplets in stagnant air. *J. Meteorol.* **1949**, *6*, 243–248. [[CrossRef](#)]
62. Schatzmann, M.; Europäische Wissenschaftsstiftung. *Proceedings/International Workshop on Quality Assurance of Microscale Meteorological Models Cost Action 732 in Combination with the European Science Foundation at Hamburg, Germany, July 28/29 2005*; University of Hamburg: Hamburg, Germany, 2005; ISBN 3000183124.
63. Best, A.C. The Size Distribution of Raindrops. *Q. J. R. Meteorol. Soc.* **1950**, *76*, 16–36. [[CrossRef](#)]
64. Blocken, B.; Carmeliet, J. Spatial and Temporal Distribution of Driving Rain on a Lowrise Building. *Wind Struct.* **2002**, *5*, 441–462. [[CrossRef](#)]
65. Bruse, M.; Huttner, S. Numerical Modeling of the Urban Climate—a Preview on ENVI-Met 4.0. In Proceedings of the 7th International Conference on Urban Climate ICUC-7, Yokohama, Japan, 29 June–3 July 2009.
66. Simon, H.; Heusinger, J.; Sinsel, T.; Weber, S.; Bruse, M. Implementation of a Lagrangian Stochastic Particle Trajectory Model (LaStTraM) to Simulate Concentration and Flux Footprints Using the Microclimate Model ENVI-Met. *Atmosphere* **2021**, *12*, 977. [[CrossRef](#)]
67. Zölch, T.; Maderspacher, J.; Wamsler, C.; Pauleit, S. Using Green Infrastructure for Urban Climate-Proofing: An Evaluation of Heat Mitigation Measures at the Micro-Scale. *Urban For. Urban Green.* **2016**, *20*, 305–316. [[CrossRef](#)]
68. Thomsit-Ireland, F.; Essah, E.A.; Hadley, P.; Blanuša, T. The Impact of Green Facades and Vegetative Cover on the Temperature and Relative Humidity within Model Buildings. *Build. Environ.* **2020**, *181*, 107009. [[CrossRef](#)]
69. Peng, L.L.H.; Jiang, Z.; Yang, X.; Wang, Q.; He, Y.; Chen, S.S. Energy Savings of Block-Scale Facade Greening for Different Urban Forms. *Appl. Energy* **2020**, *279*, 115844. [[CrossRef](#)]
70. Jänicke, B.; Meier, F.; Hoelscher, M.-T.; Scherer, D. Evaluating the Effects of Façade Greening on Human Bioclimate in a Complex Urban Environment. *Adv. Meteorol.* **2015**, *2015*, 747259. [[CrossRef](#)]
71. Ling, T.-Y. Rethinking Greening the Building Façade under Extreme Climate: Attributes Consideration for Typo-Morphological Green Envelope Retrofit. *Clean. Circ. Bioeconomy* **2022**, *3*, 100024. [[CrossRef](#)]
72. Alsaad, H.; Hartmann, M.; Hilbel, R.; Voelker, C. The Potential of Facade Greening in Mitigating the Effects of Heatwaves in Central European Cities. *Build. Environ.* **2022**, *216*, 109021. [[CrossRef](#)]
73. Shi, L.; Tao, L.; Zhang, Y.; Li, Y.; Jiang, X.; Yang, Z.; Qi, X.; Qiu, J. CFD Simulations of Wind-Driven Rain on Typical Football Stadium Configurations in China’s Hot-Summer and Cold-Winter Zone. *Build. Environ.* **2022**, *225*, 109598. [[CrossRef](#)]
74. Peng, L.L.H.; Jiang, Z.; Yang, X.; He, Y.; Xu, T.; Chen, S.S. Cooling Effects of Block-Scale Facade Greening and Their Relationship with Urban Form. *Build. Environ.* **2020**, *169*, 106552. [[CrossRef](#)]
75. Wong, N.H.; Tan, A.Y.K.; Tan, P.Y.; Wong, N.C. Energy Simulation of Vertical Greenery Systems. *Energy Build.* **2009**, *41*, 1401–1408. [[CrossRef](#)]
76. Wang, W.T.; Yang, H.; Xiang, C.Y. Green Roofs and Facades with Integrated Photovoltaic System for Zero Energy Eco-Friendly Building—A Review. *Sustain. Energy Technol. Assess.* **2023**, *60*, 103426. [[CrossRef](#)]

Disclaimer/Publisher’s Note: The statements, opinions and data contained in all publications are solely those of the individual author(s) and contributor(s) and not of MDPI and/or the editor(s). MDPI and/or the editor(s) disclaim responsibility for any injury to people or property resulting from any ideas, methods, instructions or products referred to in the content.